



A novel network training approach for open set image recognition

Md Tahmid Hossain^{a,**}, Shyh Wei Teng^a, Guojun Lu^a, Ferdous Sohel^b

^a*School of Science, Engineering and Information Technology, Federation University, Gippsland Campus, Churchill, VIC 3842, Australia*

^b*Discipline of Information Technology, Murdoch University, Perth, WA 6150, Australia*

ABSTRACT

Convolutional Neural Networks (CNNs) are commonly designed for closed set arrangements, where test instances only belong to some ‘Known Known’ (KK) classes used in training. As such, they predict a class label for a test sample based on the distribution of the KK classes. However, when used under the Open Set Recognition (OSR) setup (where an input may belong to an ‘Unknown Unknown’ or UU class), such a network will always classify a test instance as one of the KK classes even if it is from a UU class. As a solution, recently, data augmentation based on Generative Adversarial Networks (GAN) has been used. In this work, we propose a novel approach for mining a ‘Known Unknown Trainer’ or KUT set and design a deep OSR Network (OSRNet) to harness this dataset. The goal is to teach OSRNet the essence of the UUs through KUT set, which is effectively a collection of mined “hard Known Unknown negatives”. Once trained, OSRNet can detect the UUs while maintaining high classification accuracy on Kks. We evaluate OSRNet on six benchmark datasets and demonstrate it outperforms contemporary OSR methods.

© 2021 Elsevier Ltd. All rights reserved.

1. Introduction

An image classifier is expected to correctly classify images belonging to the ‘Known Known’ (KK) distribution seen during training. However, during inference, ‘Unknown Unknown’ (UU)¹ instances might trigger incorrect classification. As the training set comprises of a finite number of classes, identifying a UU instance is a challenge (see Figure 1). This is referred to as the Open Set Recognition (OSR) problem. To better understand the importance of OSR, let us consider an example. Imagine an autonomous car is trained to recognize 10 different street signs, and the car responds according to a pre-defined set of rules. The on-board sensors perceive the environment and feed data to the trained classifier (e.g., Convolutional Neural Network or CNN). In an environment full of objects beyond the closed set training classes, it is likely for a CNN to classify a non-street sign object as one of the 10 street signs (e.g., a commercial billboard might be incorrectly perceived as a stop sign). Such an event and the consequent pre-programmed response of

the autonomous car can lead to an undesired situation, even to a fatal accident.

In traditional classification tasks, a deep network is usually trained only on a KK dataset D_{KK} without considering the unknowns. For an effective OSR, training a network with ‘everything else’ in the world as the unknown is unrealistic. Therefore, a Known Unknown Trainer (KUT) dataset (referred to as D_{KUT} hereafter) is required for this task. Generative Adversarial Network (GAN)-based artificial images have often been used as a data augmentation-based solution in a number of contemporary works (Perera et al., 2020; Neal et al., 2018; Ge et al., 2017). However, being trained on only KK samples, the distribution of the augmented data is not always compatible with the UU distribution present in the test set. Moreover, GANs suffer from a number of issues stemming from the generation techniques themselves, such as unwanted artefacts, and mode collapse (Goodfellow, 2016). These deteriorate the network’s performance and increase training time. Another way to address the OSR problem is to find an effective SoftMax threshold to reject UUs (Bendale and Boulton, 2016; Oza and Patel, 2019; Ge et al., 2017).

In this work, we argue that drawing a boundary between the KK and the unknown is the key to efficiently handling the OSR task and we aim to approximate such a decision boundary by

^{**}Corresponding author [Paper under review]

e-mail: mt.hossain@federation.edu.au (Md Tahmid Hossain)

¹Note that we refer to the collection of Known Unknowns (KUs) and Unknown Unknowns (UUs) as unknowns.

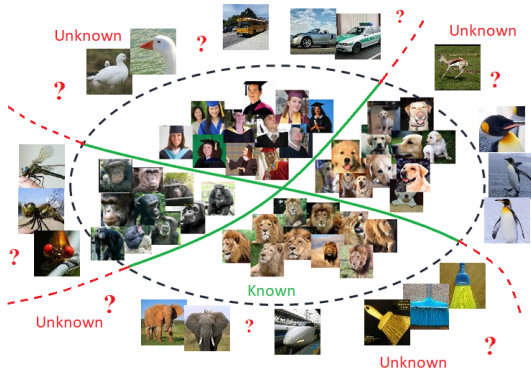


Fig. 1: Conceptual illustration of a 4-class classifier decision boundary. A deep CNN can produce high-precision classification results so long a novel test instance belongs to one of the KK classes. However, when the CNN is exposed to UU instances, it misclassifies such images as one of the KK classes because of its lack of precision outside the KK distribution.

mining a D_{KUT} . To accomplish this, we propose a way of mining the hard KU negatives into D_{KUT} and design a deep network to be trained on this dataset. D_{KUT} is mined from publicly available benchmark datasets (D_x) (where, $D_{KUT} \subset D_x$). Images from D_x inducing high probability ($P >$ some threshold T) for one of the KK classes gets admission into D_{KUT} (calculation of T is explained in Section 3). We demonstrate that OSRNet, which is trained to distinguish D_{KUT} from D_{KK} can identify novel UU instances at test time. D_{KUT} does not include any of the classes present in the UU test fold to ensure a fair evaluation.

The proposed OSRNet has two parts: a traditional CNN as the base and a Confidence Subnetwork or CS. The CNN is trained conventionally to classify a given D_{KK} . The CS, which effectively is an Artificial Neural Network (ANN), is separately trained to identify UUs. Once CS is trained, it is augmented to the trained CNN, and OSRNet is formed (details in Section 3). At inference time, the newly formed network works as one single end-to-end unit. Inside OSRNet, the CNN produces class predictions and at the same time, the CS outputs a single confidence score $S = [0, 1]$ to indicate whether an instance belongs to one of the KKs or not ($S \rightarrow 1$ denotes a high chance of the input being UU). A cut-off value δ is used on S to determine the final outcome, i.e., whether to accept or reject the class label produced by the base CNN. OSRNet does not require any additional computation module (e.g., EVT) outside the deep network’s perimeter. The entire inference process is end-to-end without any bottleneck.

The OSRNet architecture is inspired from the observation by Bendale et al. (Bendale and Boult, 2016) depicted in Figure 2. It is reported that when classifying an image from D_{KK} , traditional CNNs generally produce a high probability score for the correct class while the leftover probability is usually distributed across visually similar classes. Even when a CNN is unsure or misclassifies a KK instance, the probability scores mostly remain concentrated to visually similar classes. In contrast, when an unknown instance gets classified as one of the KK classes, the leftover probability distribution does not usually follow such a pattern (Bendale and Boult, 2016). For illus-

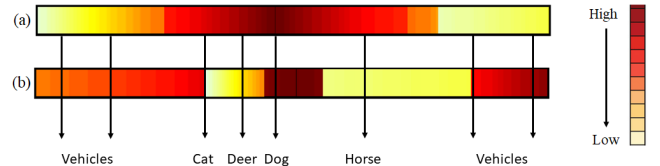


Fig. 2: Behavioural difference of a trained CNN on classes it has and has not seen during training. For a KK test instance, usually, the correct class receives maximum probability, and the leftover energy is distributed to visually similar classes. In contrast, no such pattern is found for an Unknown test instance. (a) denotes the probability heat map for CIFAR-10 dog class (test set). Most of the energy is distributed to either dog or among classes visually similar to dog, e.g., cat, deer, and horse. In (b), when unknown instances (taken from CIFAR-100) are misclassified as dog, the leftover energy distribution does not follow the same pattern.

tration (in Figure 2), we train a simple CNN on CIFAR-10 and generate a probability heat map for the dog class test set. It is evident in Figure 2(a) that either dog or classes visually similar to dog receives most of the energy. In Figure 2(b), we feed the same CNN instances from unseen CIFAR-100 classes and produce the heat map with 1,000 samples misclassified as dog. The leftover probability distribution has marked contrast to Figure 2(a). This is the pattern we aim to exploit in this work for OSR. Because of the above-mentioned behavioural difference on KKs and any Unknown instances, we expect the intermediate layer features (Fully Connected or FC) of a CNN (trained on D_{KK}) to reflect this difference. Therefore, FC features should be distinct for KK and unknown samples. Collecting such FC features for D_{KK} is straightforward from our base CNN. However, mining an appropriate D_{KUT} set to collect FC features is challenging. Our proposed method addresses both issues.

In this work, we make the following contributions:

- We propose a way of building the Known Unknown Trainer dataset D_{KUT} for OSR.
- To effectively distinguish between the KKs from the UUs at test time, a novel deep network (OSRNet) is proposed.
- We extensively evaluate OSRNet and compare with contemporary OSR methods on six benchmark datasets. OSRNet not only detects UUs with higher precision but also exhibits impressive discriminative power within D_{KK} .
- Finally, we discuss the underlying reasons behind the effectiveness of the proposed D_{KUT} and OSRNet in OSR.

The rest of the paper is organized as follows: Section 2 discusses the relevant works. In Section 3, we demonstrate the architecture of the proposed OSRNet, D_{KUT} mining process, how an effective threshold T is chosen as the selection criteria and why it works so well. In Section 4, we outline the datasets used for training and testing and implementation details. Section 5 provides an experimental evaluation of the proposed and existing methods. Section 6 provides a discussion on the Known Unknown Trainer image set. Finally, Section 7 concludes this paper.

2. Related Work

Open Set Recognition. OSR methods can be categorized into two main types: CNN-based and non-CNN-based. Scheirer et al. (Scheirer et al., 2012; Scheirer et al.) first formalized the OSR problem and proposed an SVM-based solution. Extreme Value Theory (EVT) is used in a number of works (Rudd et al.; Zhang and Patel) to reject UU instances receiving probability score lower than a threshold. Dang et al. (Dang et al., 2019) proposed an OSR model where edge exemplars are selected for every class based on local geometrical and statistical properties (Li and Maguire, 2010). Later, EVT-based rejection rule is adopted to reject any UU input that lies outside the KK class boundaries. Recently, deep learning-based networks are found to be more effective in OSR.

OSR with Counterfactual Images (OSRCI) (Neal et al., 2018) uses GAN to produce Counterfactual Images (CI) by morphing instances from D_{KK} to an extent where they no longer are recognizable as a true class object (neither KK nor unknown). Later, these CI are used as the D_{KUT} (i.e., $CI \approx D_{KUT}$). An additional $(N + 1)^{\text{th}}$ ‘other’ class is introduced to accommodate images in D_{KUT} during training. At inference time, the classifier is expected to classify UU instances as ‘other’. Although the network is expected to classify real-world objects, CI used as D_{KUT} lack visual characteristics of natural images limiting the effectiveness of OSRCI.

Bendale et al. (Bendale and Boulton, 2016) replaced the SoftMax function with OpenMax. It is argued that forcing a network’s total output probability to sum up to 1 leads the network to put undue probability score to UU instances at test time. It has been reported that test instances from D_{KK} put high prediction scores on the true class while the leftover probability is distributed to visually similar classes. However, the output probability distribution does not exhibit the same pattern for unknown instances. Inspired from this observation, the penultimate layer features (Activation Vector or AV) are extracted, and a mean vector (AVM) is calculated for each class (class-wise images are fed to the CNN). At test time, the AV of an image is extracted, and its distances to all the AVMs are calculated. Later, these distances are used with a threshold to detect whether the image belongs to a KK class or not. Ge et al. (Ge et al., 2017) supplemented OpenMax with Generative OpenMax (G-OpenMax) where they used GAN-generated data for OSR training. Classification-Reconstruction learning for Open-Set Recognition (CROSRL) (Yoshihashi et al., 2019) is also an extension of OpenMax, but a different route is followed. A two-part deep network is used: a KK classifier and a UU detector. Multiple intermediate layers of the main CNN classifiers are treated as latent features, and a decoder is used to reconstruct the input. The UU detector and the classifier, both exploit the latent space features jointly to output detection decision and class label respectively.

Class Conditioned Auto-Encoder (C2AE) (Oza and Patel, 2019) also adopts an Encoder Decoder-based reconstructive approach. An encoder network is first trained on D_{KK} , and the penultimate layer is used as the encoded vector (EV). For each class in D_{KK} , one such EV is stored as the class condition vector. A decoder is later used to reconstruct the input from the EV. For

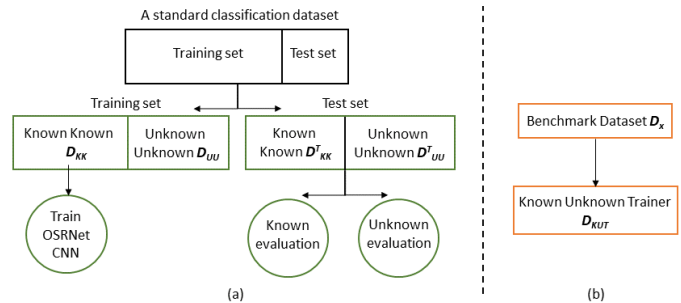


Fig. 3: (a) An overview of the dataset splits in this work. (b) The Known Unknown Trainer dataset D_{KUT} is a subset of D_x mined following our proposed method. D_{KUT} does not contain any of the D'_{UU}/D_{UU} classes. As a result, OSRNet remains blind regarding the classes it is going to encounter during evaluation.

each input to the encoder, the EV output is compared against all the stored EVs. The decoder reconstructs the input as perfectly as possible whenever a match is found between the output and stored EVs. However, for UU images (with no EV matches), the decoder is designed to perform a poor reconstruction so that the reconstruction error is high at inference time. C2AE is not an end-to-end unit and leaves room for further improvement.

Geng et al. (Geng et al., 2020) proposed a visual and semantic prototypes-jointly guided CNN (VSG-CNN) to achieve the task of OSR. Instead of using traditional cross-entropy loss, a distance-based cross-entropy loss (DCE) is used to find out the probability of a test instance belonging to each KK class. Once this probability set is at hand, the overall entropy is calculated and based on a threshold, the test instance is either rejected as a UU class or classified as one of the KK ones.

Out-of-Distribution Detection. Out-of-Distribution (OOD) or Anomaly Detection is correlated to OSR. OSR deals with identifying real but UU images while classifying any KK instance. On the other hand, OOD detectors focus on anomalous outlier detection. Sometimes, these anomalies can be visually unrecognizable (Nguyen et al., 2015) or ‘rubbish’. Some methods only detect the outliers first, and a separate classifier is used later for classification only if an input is deemed as KK by the detector (Liang et al., 2018; Vyas et al., 2018).

A common way to tackle the OOD problem is to simply augment an additional class to an existing CNN so that all OOD instances are classified as the ‘other’ class (Grosse et al., 2017). However, adding an additional class for all other images in the world do not perform consistently well on different benchmark datasets (Nguyen et al., 2015). Hendrycks et al. (Hendrycks and Gimpel, 2016) used the SoftMax probabilities as a heuristic to detect outlier images. A simple thresholding technique is applied based on the assumption that in distribution samples will always have higher probabilities, and OOD instances would not trigger high confidence predictions. However, this assumption is inaccurate. SoftMax thresholding does not work well as CNNs often misclassify an OOD image with high probability. As a solution, some detection methods introduce OOD samples in the training data and employ a custom loss function to uniformly diffuse probability on OOD training samples (Hendrycks et al., 2019; Hein et al., 2019; Lee et al., 2017;

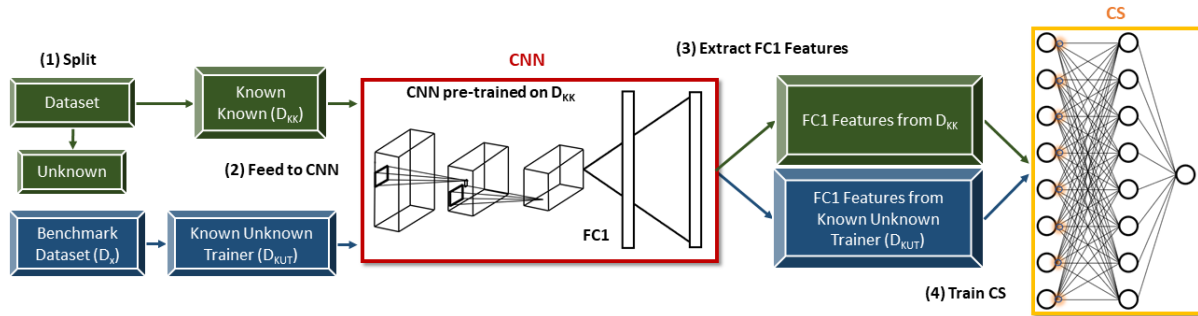


Fig. 4: An overview of OSRNet training process. A CNN ($ResNet_{2FC}$) is trained on the KK split (D_{KK}) of a dataset. Images from D_{KK} and D_{KUT} mined from another benchmark dataset D_x is fed to this already trained CNN. FC_1 features are extracted for both D_{KK} and D_{KUT} and the CS is trained with these features and binary labels. Once trained, this CS is augmented to the corresponding CNN layer (FC_1) and the proposed OSRNet is formed. At inference time, OSRNet works as one single end-to-end unit. The augmented CS receives FC_1 features from the CNN and detects whether the input belongs to one of the D_{KK} classes or not. The CNN, on the other hand, simultaneously classifies an instance without any interference from the CS.

DeVries and Taylor, 2018). These loss functions constrain the CNN from wrong overconfident predictions, but overall accuracy is compromised. Moreover, These methods use one benchmark dataset as D_{KK} and other entire publicly available benchmark datasets (Hendrycks et al., 2019) (D_x) as D_{KUT} (i.e., $D_x \approx D_{KUT}$). We argue that mining only the hard known unknown negatives from D_x into D_{KUT} works better (i.e., $D_{KUT} \subset D_x$).

Li et al. (Li and Li, 2017) investigated the statistical properties of different CNN layer features to find a distinguishing pattern between In and Out of Distribution images. It is reported that the convolution outputs for D_{KK} and OOD instances have subtle difference. The difference is so subtle that even the most impactful dimensions in PCA (PCA head) fail to capture the difference. However, the tail (less informative eigen dimensions) of PCA shows a difference in the pattern. These features are used to train a cascade classifier for OOD detection.

GAN is used for OOD (Hein et al., 2019; Mandal et al., 2019; Lee et al., 2017; Ge et al., 2017; Neal et al., 2018). Lee et al. (Lee et al., 2017) used GAN to produce a D_{KUT} that neither belongs to D_{KK} , nor lies far away. A custom loss function (L) based on Kullback-Leibler divergence between a uniform distribution U and prediction on OOD instances is used for probability diffusion.

3. Proposed Method

3.1. OSRNet

Before elaborating on the proposed method, we outline the dataset splits for convenience:

- **(Training)** One KK set D_{KK} .
- **(Training)** One Known Unknown Trainer set D_{KUT} mined from a D_x following our proposed method (details in Section 3.2).
- **(Test)** One KK test set D_{KK}^T .
- **(Test)** One UU test set D_{UU}^T .

Following the evaluation process defined in (Neal et al., 2018; Oza and Patel, 2019), we split a standard classification

Table 1: An empirical analysis of OSRNet’s performance on different D_{KUT} selection criteria or threshold T . It is evident that images from D_x with $P \geq 80\%$ perform best as D_{KUT} . The average entropy is also the lowest around this point.

KK			D_x (AUROC %)				
	Probability Threshold (%)	Entropy $H(X)$	CIFAR100	Indoor67	Caltech256	T-ImageNet	F-MNIST + ADBase
CIFAR10	60	1.65	75.60	69.25	78.65	78.23	-
	70	1.41	78.85	75.02	84.30	82.30	-
	80	1.10	89.25	83.82	93.15	88.40	-
	90	1.21	86.32	81.40	89.66	85.49	-
CIFAR+10	60	1.71	-	72.69	80.20	80.60	-
	70	1.45	-	79.05	88.54	84.25	-
	80	0.98	-	85.76	95.69	91.40	-
	90	1.16	-	82.85	92.36	88.71	-
CIFAR+50	60	1.55	-	71.15	83.69	77.06	-
	70	1.51	-	79.30	90.04	84.55	-
	80	1.18	-	83.60	94.60	89.78	-
	90	1.24	-	80.95	92.69	87.45	-
T-ImageNet	60	1.92	60.88	55.01	62.22	-	-
	70	1.64	69.35	65.25	73.41	-	-
	80	1.36	74.55	70.95	77.10	-	-
	90	1.48	72.98	68.07	75.94	-	-
MNIST	60	1.33	-	-	-	-	93.42
	70	1.18	-	-	-	-	95.36
	80	0.91	-	-	-	-	98.96
	90	1.08	-	-	-	-	96.25
SVHN	60	1.47	-	-	-	-	88.40
	70	1.21	-	-	-	-	91.13
	80	1.02	-	-	-	-	92.66
	90	1.14	-	-	-	-	90.69

dataset (e.g., CIFAR10) into a KK part D_{KK} and a UU part D_{UU} . D_{UU} is left aside and only its test set counterpart D_{UU}^T is used for evaluation along with D_{KK}^T . D_{UU}^T is used only for testing and our network remains unaware of the classes contained in D_{UU}^T . A Known Unknown Trainer set D_{KUT} is mined from another publicly available benchmark dataset D_x . Classes contained in either D_{KK} or D_{UU}^T are removed from D_x so that D_{KUT} does not contain any overlapping classes ($D_{KK} \cap D_{UU}^T \cap D_{KUT} = \emptyset$). Figure 3 provides an overview of the dataset splits.

OSRNet consists of two parts: a base CNN is responsible for classifying an instance (x) regardless of its distribution, i.e., KK or UU. On the other hand, the CS augmented to the base CNN outputs a score indicating whether $x \in D_{KK}$ or $x \notin D_{KK}$ (see Figure 4). In other words, even if an input belongs to a class that our network has not seen during training, the CNN will output a label. It is up to the CS to decide whether to accept or reject it. To put these formally, an input image x triggers the N -way CNN in OSRNet (N is the number of classes) to produce a probability y_i ($i \in \{1 \dots N\}$) for each of the classes. The CS

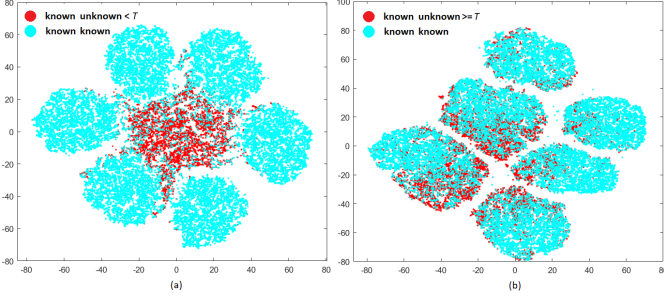


Fig. 5: t-SNE plots of (a) FC_l features from all images in D_{KK} (cyan) and those in D_x (red) inducing probability $P <$ some threshold T and (b) $P \geq T$. It is visually evident that separating KUs from KUs in (b) is more difficult. OSRNet trained to separate KUs from KUs in (b) can identify relatively easier KUs in (a) as well. An effective probability threshold T is chosen based on finding the maximum point on a cubic polynomial curve (see Figure 6).

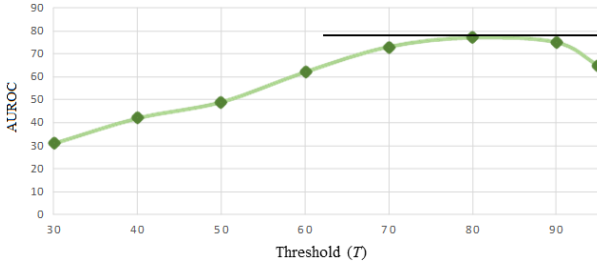


Fig. 6: AUROC vs T curve based on sample points for Tiny ImageNet as D_{KK} and Caltech256 as D_x . A probability threshold T is calculated from the maximum point on the curve. This threshold T calculation is repeated for each D_{KK} reported in this work.

outputs a score S for each x , indicating the confidence of the input being a UU instance. The final OSRNet output OP can be expressed using Equation 1.

$$OP = \begin{cases} \max P(y_i|x) & \text{if } S < \delta, \\ x \notin D_{KK} & \text{else} \end{cases} \quad (1)$$

where, $i \in \{1 \dots N\}$

As shown later, an optimally chosen cut-off value δ can be applied on S to reject UU instances.

As discussed in Section 1 and depicted in Figure 2, the probability scores of a CNN are confined within the visually similar classes when the input belongs to D_{KK} . However, the probability distribution does not follow the same trend for unknown instances. Therefore, the intermediate layer features of a CNN should exhibit differences for the KK and unknown classes. Since we aim to exploit this behavioural distinction, the choice of the feature layer is important. In contrast to a single Fully Connected Layer (FC_{Soft}) used in traditional ResNet (we call it ResNet_{1FC}) (He et al., 2016), we add one additional FC Layer (FC_l) prior to FC_{Soft} and train this ResNet (we call it ResNet_{2FC}) on D_{KK} from scratch. A detailed analysis on the impact of different ResNet variants and OSRNet’s performance is provided in Section 5.

3.2. Known Unknown Trainer Dataset Mining

After splitting a standard classification dataset into D_{KK} and

D_{UU} , ResNet_{2FC} is trained on D_{KK} and remains completely unaware of the classes in D_{UU} . To mine D_{KUT} , another publicly available benchmark dataset D_x is fed to a ResNet_{2FC} trained on D_{KK} . From all the images in D_x , only the ones inducing probability greater than a threshold are mined for D_{KUT} , i.e., $\forall x \exists(x) (P(x) > T)$ (see Figure 5). Choosing an effective T is vital for OSRNet’s performance. To select such a T , it is important to analyze how different T values fare against OSRNet’s performance. Table 1 has a compilation of increasing T against Area Under ROC curve or AUROC score of OSRNet. It is evident that for the given sample points, $T \approx 80\%$ is a good choice across datasets. Calculating OSRNet’s performance on every possible T is tedious. Therefore, to pick a T , we fit a cubic polynomial curve for all the collected sample points across datasets (e.g., (70, 78.85) is a data point for CIFAR10 (D_{KK})-CIFAR100 (D_{KU}) combination). The curve is represented by Equation 2 (A, B, C, and D are coefficients).

$$F(T) = A + BT + CT^2 + DT^3 \quad (2)$$

A degree two quadratic function has a higher error rate than a cubic one and hence we fit a cubic curve approximated by Equation 2 (see Figure 6). With the help of first and second-order derivatives, the maximum point on the curve is found where the gradient of a tangent to the curve $F(T)$ is 0. We fit an AUROC vs T curve for all the D_{KK} s with Caltech256 as the D_x (as will be explained in the next section, Caltech256 is the best D_x). For each D_{KK} and D_x , a threshold T is calculated from the curve.

Key characteristics of this curve (Figure 6) are explained below:

- A smaller T allows a large number of images from D_x to qualify for D_{KUT} . A considerably small T might allow the entire D_x set to qualify for D_{KUT} (i.e., $D_x \approx D_{KUT}$ if $T \rightarrow 0$). As a result, D_{KUT} gets populated with sub-optimal imagery along with high probability inducing ones. OSRNet’s performance (AUROC), upto a certain point, improves with increasing T .
- OSRNet’s performance experiences a downward trend followed by the peak ($T \approx 80\%$). This is because too high of a T value leaves very few images from D_x to be eligible for D_{KUT} . Such a D_{KUT} is inadequate as training dataset for OSRNet. Hence, OSRNet’s performance drops as the meagre training data in D_{KUT} leads to overfitting.
- OSRNet’s performance peaks around $T \approx 80\%$ for all the datasets. Such a T offers the best trade-off between the number and quality of images mined for D_{KUT} .

Algorithm 1 summarizes the overall D_{KUT} mining process, which is used to teach OSRNet the essence of the UU world. For numeric datasets such as MNIST and SVHN as D_{KK} , the options for an ideal D_x are limited because natural object classes do not work well as D_x for such numeric D_{KK} s. In this work, Fashion MNIST (Xiao et al., 2017) and ADBase (El-Sherif and Abdelazeem, 2007) are used in conjunction as the base D_x .

Algorithm 1 : D_{KUT} Construction Process

Input: Images (x_n) from D_x , $n \in N$, N is the total number of images in D_x .

Output: x_n either selected or discarded for D_{KUT} .

```

1: Choose a benchmark dataset as the base  $D_x$ 
2: for all  $x_n \in D_x$ , where  $n = \{1, 2, \dots, N\}$  do
3:   Feed  $x_n$  to  $ResNet_{2FC}$ 
4:    $p = \max(Probability(x_n))$ 
5:   if  $p > T$ , where  $T$  is an optimal threshold found from the
     curve in Equ. 2 then
6:      $D_{KUT} \leftarrow x_n$ 
7:   else
8:     Discard  $x_n$ 
9:   end if
10: end for

```

3.3. Training OSRNet

Training OSRNet involves a series of steps. The overall training workflow is depicted in Figure 4, and the steps are explained below.

- ResNet_{2FC} is used to extract FC_1 features from the same D_{KK} it was initially trained on. All these features are labeled as 0.
- D_{KUT} images (mined following the process in Section 3.2) are fed to the same ResNet_{2FC} and FC_1 features are extracted. These features are labeled as 1.
- The CS (an ANN with one output node) is trained with these two sets of FC_1 features (from D_{KK} and D_{KUT}) to teach the difference between the KK and the UU. As the CS is capable of distinguishing relatively difficult borderline D_{KUT} features from D_{KK} features, it can identify rest of the relatively easier KUs in D_x .
- Finally, this trained CS is augmented to the corresponding (FC_1) layer of the pre-trained ResNet_{2FC}. OSRNet functions as a single unit at inference time.

Algorithm 2 summarizes the OSRNet training process. As the CS takes care of UU detection, ResNet_{2FC} within OSRNet maintains the original classification accuracy on the test fold of D_{KK} . At test time, OSRNet not only produces a class label but also provides a confidence score suggesting how likely an input is to be UU.

3.4. Why OSRNet works?

Since perceiving high dimensional space is difficult for humans, conceptual illustrations are widely used for better understanding (Dube, 2018; Tanay and Griffin, 2016). Here, with the help of Figure 7, we explain why the proposed D_{KUT} and OSRNet work well in OSR.

The asterisks within the dotted oval resemble D_{KK} , and classification within this oval is quite accurate. The negative space or the region beyond the encapsulating oval accommodates all the unknown images (as mentioned earlier, we refer to KUs + UUs as unknowns), i.e., nearby unknowns (circle), and far away

Algorithm 2 : OSRNet Training

Input: Individual images from D_{KUT} (referred x_i) and D_{KK} (referred x_j).

Output: Trained OSRNet.

```

1: for all  $x_i \in D_{KUT}$ , where  $i = \{1, 2, \dots, N\}$  do
2:   Feed  $x_i$  to  $ResNet_{2FC}$ 
3:    $Feature_{KUT}[i] \leftarrow FC_1$ 
4:    $Feature_{KUT\_label}[i] \leftarrow 0$ 
5: end for
6: for all  $x_j \in D_{KK}$ , where  $j = \{1, 2, \dots, N\}$  do
7:   Feed  $x_j$  to  $ResNet_{2FC}$ 
8:    $Feature_{KK}[j] \leftarrow FC_1$ 
9:    $Feature_{KK\_label}[j] \leftarrow 1$ 
10: end for
11: Train Confidence Subnetwork (CS)
     with  $\{Feature_{KUT}, Feature_{KUT\_label}\}$  and
      $\{Feature_{KK}, Feature_{KK\_label}\}$ 
12: Augment CS to  $ResNet_{2FC}$ 

```

unknowns (triangle). Traditional CNN's performance lack robustness in the negative space since the decision boundaries (dotted red) extrapolate to infinity (Goodfellow et al., 2015) without any precision. In this work, we only use high probability ($P > T$) inducing images in D_{KUT} to represent the UU. Such images (blue circles) in D_{KUT} reside close to the KK distribution (the dotted oval). We argue that a deep classifier capable of treating the borderline D_{KUT} instances (blue circles) as unknown can easily identify relatively easier far-away unknowns (triangles). It is understandably a challenging task to collect all the borderline unknowns perfectly encapsulating the KK distribution.

In this work, we strive to maximize the participation of such borderline images in D_{KUT} . A couple of follow-up questions still remain:

- (Q1) For a certain D_{KK} , which D_x should we choose to mine D_{KUT} ?
- (Q2) Can a D_{KUT} with fewer data outperform some D_x it was mined from (although $D_{KUT} \subset D_x$)?

Answer to Q1. We have experimented with four public datasets: CIFAR100, Indoor67, Clatech256, and Tiny ImageNet as D_x . It is evident from Table 1 that Caltech256 performs best as D_x across datasets and Indoor67 comes out last. One intriguing aspect is comparing the visual characteristics of the best performing D_x against others. Is it visually similar to D_{KK} ($D_x \approx D_{KK}$) or is it quite different (we show quantitative distance between different data distributions in Section 6)? For example, bus is a visually similar class to truck compared to some indoor images. It turns out, Indoor67 is not a good candidate for D_x as it consists of only interior images (e.g., office room, bedroom, and auditorium) with little to no visual similarity to the D_{KK} s. On the other hand, Caltech256 performs better as it consists of classes ranging from a variety of animals to different vehicles having greater visual similarity to the D_{KK} s.

Our suggestion is to use a D_x that has classes similar to D_{KK} . E.g., if a certain D_{KK} consists of different dog breeds, a dataset

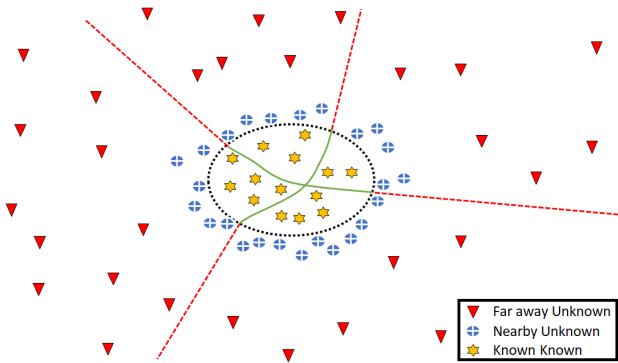


Fig. 7: A conceptual illustration of the D_{KUT} image characteristics. D_{KUT} consists of only the nearby unknowns and OSRNet is trained to detect these difficult to identify unknowns. This way, the far-away unknowns are automatically detected without being used as part of the training. For OSRNet, less training data is required and better accuracy is achieved.

containing different cat breeds could be a better option as D_x rather than using some indoor images like Indoor67 as the D_x . We argue that training to separate an apparently more difficult D_x , like Caltech256, from D_{KK} enables OSRNet to automatically distinguish relatively easier instances at test time.

Answer to Q2. Experimental analysis shows that the type of images in D_{KUT} is more important than the number of images. It is intriguing that despite being a subset of D_x , D_{KUT} teaches OSRNet the essence of the unknown world better than a much larger in size D_x . A detailed explanation of this observation is provided in Section 6.

To further understand the conceptual explanation and why mining only high probability inducing KUs for D_{KUT} makes sense, we resort to entropy comparison. In multi-class classification tasks such as ours, a trained CNN provides a class probability for each of the output nodes. The probability distribution (D_P) generated by the CNN portrays how certain the network is about the classification. When a test instance is classified confidently, one output node exhibits higher (≈ 1) probability than the rest. The uncertainty factor is low here as is the entropy. Conversely, when the classifier is susceptible to the input and does not provide a confident probability distribution (e.g., a Uniform Distribution), the uncertainty is high and hence the entropy as well. This suggests that for an input, lower the D_P uncertainty, closer the input is to D_{KK} . This uncertainty can be quantified from D_P entropy using Equation 3.

$$H(X) = H(p_1, \dots, p_n) = - \sum_{i=1}^n p_i \log_2 p_i \quad (3)$$

In a number of cases, when a trained deep CNN faces UU instances, the entropy or $H(X)$ stays low. This generally means those images are adjacent to the KK distribution despite actually being UU. On the other hand, the rest of the images induce high $H(X)$ which implies such images are generally not adjacent to D_{KK} and rightly so. As can be seen from Table 1, the lowest entropy co-occurs with the best performing T . This supports the usage of only high probability inducing images ($P > T$) in D_{KUT} since such a D_{KUT} would be closer to D_{KK}

and harder to distinguish resulting in a tight but efficient decision boundary.

4. Experiments

4.1. Datasets and splits

MNIST, SVHN, CIFAR10. MNIST (LeCun et al., 2010) is a digits dataset containing 60,000 training and 10,000 test images. Each digit from 0 to 9 denotes a class. All the images are grayscale and have a resolution of 28×28 . SVHN (Netzer et al., 2011) is also a digits dataset, but the images are collected from Google Street View cameras capturing house numbers (from 0 to 9 as well). This dataset is considered harder than MNIST and contains 32×32 colour images. It has 73,257 training and 26,032 test instances. CIFAR10 (Krizhevsky and Hinton, 2009) also has 10 classes with 32×32 colour images. It has 50,000 training and 10,000 test images of different objects (e.g., cat and dog). To train OSRNet individually, each of these three datasets is split into D_{KK} with six classes and D_{UU} with four classes. The split for corresponding test set is same as the training set, i.e., D_{KK}^T and D_{UU}^T contain same classes as their training split. For example, while training on MNIST, six randomly selected classes are used as D_{KK} and the other four classes are considered as D_{UU} . For each dataset, the ‘openness’ is estimated by Equation 4 (Scheirer et al., 2012; Neal et al., 2018). Greater openness value implies higher difference in the number of classes between D_{UU}/D_{UU}^T and D_{KK}/D_{KK}^T , i.e., the UU to KK class ratio is higher. It is worth reinstating that no images from D_{UU} is used in training OSRNet. Only the test fold D_{UU}^T is used for testing.

$$\text{openness} = 1 - \sqrt{\frac{|N|}{|Q|}} \quad (4)$$

Here, $|N|$ and $|Q|$ denote the number of D_{KK} classes and the number of total test classes ($D_{UU}^T + D_{KK}^T$) respectively. The term *openness* is measured in percentage where higher value represents greater *openness*. According to Equation 4, *openness* of CIFAR10, MNIST and SVHN is 22.50%.

CIFAR+10. Four classes from CIFAR10 are selected as D_{KK} and 10 non-overlapping classes from CIFAR100 are selected as D_{UU} . *openness* is 46.50%.

CIFAR+50. Four classes from CIFAR10 are selected as D_{KK} and 50 non-overlapping classes from CIFAR100 are selected as D_{UU} . *openness* is 72.78%.

Tiny ImageNet. Tiny ImageNet is a subset of ImageNet (Deng et al., 2009) comprising 200 classes with 64×64 colour images. Each of the classes has 500 training and 50 test images. We randomly select 20 classes as D_{KK} and 180 classes as D_{UU} . *openness* is 68.38% The class selection process is random, and for each benchmark dataset, we experiment with five iterations and the average is reported (Section 5).

4.2. Known Unknown Trainer Datasets

We use publicly available benchmark datasets (D_x) to mine D_{KUT} .

Caltech256. As explained earlier, Caltech256 performs best

as D_x for all non-digit D_{KK} s. It has 256 object categories containing 30,607 images. All the overlapping classes among D_x , D_{KK} , D_{UU} are removed to achieve a fair (no prior knowledge about D_{UU}^T) and sane (no D_{KK} class is used later in training as UU) D_{KUT} .

Fashion MNIST, ADBase. Fashion MNIST (Xiao et al., 2017) has exactly the same attributes as MNIST but contains 10 classes of fashion products. ADBase (El-Sherif and Abdelazeem, 2007) is the Arabic version of MNIST. Images in both of these datasets are of resolution 28×28 and grayscale. These two datasets are used collectively as the D_x for both of the numeric datasets, i.e., when D_{KK} belongs to either MNIST or SVHN.

4.3. Training CNN

CIFAR10, CIFAR+10, CIFAR+50, SVHN. Each of these datasets has 32×32 colour images. After splitting the datasets into D_{KK} and D_{UU} following the process described in the previous section, a CNN classifier is trained on D_{KK} . ResNet_{2FC} (with depth 20 (He et al., 2016)) is used as the CNN in OSRNet. The first 3×3 convolution layer is followed by six $3 \times 3 \times 16$, six $3 \times 3 \times 32$ and six $3 \times 3 \times 64$ convolution layers where the first two dimensions represent the filter size and the third dimension stands for the number of filters. The SoftMax output is preceded by an N -way (N is the number of classes in D_{KK}) FC_{Soft} layer. FC_{Soft} layer in turn is preceded by the additional FC_1 layer.

Tiny ImageNet. ResNet_{2FC} (with depth 32 (He et al., 2016)) is used to train on D_{KK} of Tiny ImageNet. It has six $3 \times 3 \times 16$, $3 \times 3 \times 32$, six $3 \times 3 \times 64$, six $3 \times 3 \times 128$, and $3 \times 3 \times 256$ convolution layers. The FC_{Soft} layer here as well, is preceded by an additional FC_1 layer. Since images in this dataset has a higher spatial resolution, a deeper variant of ResNet_{2FC} is used.

The greater distinctiveness of the additional FC_1 features from ResNet_{2FC} compared to solitaire FC_{Soft} features in ResNet aids OSRNet’s open set recognition performance. The benefits come at a negligible increase in the total number of network parameters ($\approx 3.5\%$). Detailed results are provided in Section 5.

MNIST. For MNIST, we train a plain CNN on D_{KK} consisting of three 3×3 convolution blocks with respective filter numbers of 8, 16, and 32. These layers are followed by two FC layers (128 unit FC_1 and N -way FC_{Soft}) and the SoftMax output layer. ResNet architecture is not adopted for MNIST as a plain CNN network works just fine with competitive classification accuracy (99.66%).

We adopted stochastic gradient descent (SGD), data shuffling before every epoch while training and data augmentation (horizontal flip and translation). Minibatch size of 128 is used for all the datasets except MNIST (8,192). Adaptive dropout (Hosain et al., 2019) is followed to avoid overfitting. A multi-class cross-entropy loss (\mathcal{L}_m) is used as the objective function (Equation 5).

$$\mathcal{L}_m = - \sum_{i=1}^N \sum_{j=1}^K t_{ij} \ln y_{ij} \quad (5)$$

where N is the number of samples, K is the number of classes, t_{ij} denotes that the i^{th} sample belongs to the j^{th} class, and y_{ij} is the output for sample i for class j , which effectively is the value from the SoftMax function, i.e., it is the probability that the network associates the i^{th} input with class j .

4.4. Training CS

As depicted earlier in Figure 4, CS is an ANN subnetwork within OSRNet and is responsible for detecting UUs while ResNet_{2FC} classifies the instance. Features (for D_{KK} and D_{KUT}) extracted from ResNet_{2FC}’s FC_1 layer are fed to CS as the training data. Binary class labels are supplied as the ground truth and variable learning rate gradient descent (GDX) with momentum is used as the training method. We train CS with two hidden layers and the number of hidden units (H) per layer is between the number of inputs and outputs (Blum, 1992). For 128 dimensional FC_1 features, H is set to 64, 128, and 256 while for 256 dimensional FC_1 features, H is set to 128, 256, and 512. A binary cross-entropy loss function (\mathcal{L}_b) is used following Equation 6.

$$\mathcal{L}_b = - \frac{1}{N} \sum_{i=1}^M T_i \log(Y_i) \quad (6)$$

where M is the total number of responses in Y , N is the total number of observations in Y , Y_i is the network output, and T_i is the target value.

For each configuration, 10-fold training is conducted. Later, the best average score yielding CS is augmented to the corresponding ResNet_{2FC} to form OSRNet. It is observed that, CS with H as 64 performs best for 20-depth ResNet_{2FC} and CS with H as 128 performs best for 32-depth ResNet_{2FC}. Hence the reported results in Table 2 are derived using these two ensembles.

4.5. Optimum Confidence Cut-Off δ Estimation

Area Under the ROC curve provides an overview of a binary classifier’s performance. A greater AUROC magnitude indicates better performance. However, when the classifier is deployed in a real-life application, it is expected to rule out negative samples based on a cut-off value δ . A classifier’s ultimate accuracy largely depends on the choice of δ . An optimal δ ensures maximum correct classification with minimum error. Such a δ can be estimated from the optimal operative point on the ROC curve. There are multiple ways of finding such a point on ROC curve that will provide a good compromise between FPR ($1 - \text{specificity}$) and TPR (sensitivity). However, in this work, we follow the optimal slope intersection method (Swets, 1992; Zweig and Campbell, 1993) where an initial slope S_{op} is calculated in the ROC curve from the misclassification cost using Equation 7.

$$S_{op} = \frac{C(P|N) - C(N|N)}{C(N|P) - C(P|P)} \times \frac{N}{P} \quad (7)$$

$C(N|P)$ is the cost of misclassifying a positive class as a negative class. $C(P|N)$ is the cost of misclassifying a negative class as a positive class. In our case, the cost of any form of misclassification is equally penalized ($C(N|P) = C(P|N) = 0.5$). On

Table 2: AUROC performance (%) comparison of different OSR and OOD methods.

Method	CIFAR10	CIFAR+10	CIFAR+50	MNIST	SVHN	Tiny ImageNet
SoftMax	67.70	81.60	80.50	97.80	88.60	57.70
OpenMax (Bendale et al. (Bendale and Boulton, 2016))	69.50	81.70	79.60	98.10	89.40	57.60
G-OpenMax (Ge et al. (Ge et al., 2017))	67.50	82.70	81.90	98.40	89.60	58.00
OSRCI (Neal et al. (Neal et al., 2018))	69.90	83.80	82.70	98.80	91.00	58.60
C2AE (Oza et al. (Oza and Patel, 2019))	89.50	95.50	93.70	98.90	92.20	74.80
OE (Hendrycks et al. (2019))	63.50	73.40	71.20	93.11	81.40	44.90
ODIN (Liang et al. (2018))	64.10	75.10	72.20	96.10	81.30	47.10
G-ODIN (Hsu et al. (2020))	68.80	79.10	73.20	97.40	84.70	47.30
Proposed Method (D_K)	90.40 ± 0.08	94.88 ± 0.12	93.50 ± 0.11	98.35 ± 0.09	91.22 ± 0.14	75.70 ± 0.20
Proposed Method (D_{KUT} -ResNet1FC)	91.66 ± 0.05	94.95 ± 0.08	94.03 ± 0.10	98.44 ± 0.05	91.45 ± 0.10	76.80 ± 0.16
Proposed Method (D_{KUT}-ResNet2FC)	93.15 ± 0.04	95.69 ± 0.06	94.60 ± 0.07	98.96 ± 0.04	92.66 ± 0.09	77.10 ± 0.13

Table 3: Classification accuracy (%) comparison of contemporary OSR methods. OSRNet₁ is the variant of OSRNet with ResNet_{1FC}.

CIFAR10 D_{KK}				
OSRNet ₁	OSRNet	OpenMax	G-OpenMax	OSRCI
80.20	82.91	80.10	81.60	82.10
MNIST D_{KK}				
99.50	99.72	99.50	99.60	99.60
SVHN D_{KK}				
94.61	95.95	94.70	94.80	95.10

Table 4: Classification accuracy (%) comparison among traditional ResNet_{1FC}, ResNet_{2FC}, and ResNet_{3FC}. ResNet_{2FC} performs better on the benchmark classification task (without KK-UU split). Tiny ImageNet does not have labeled test set hence not shown here.

Classification Accuracy (%)	CIFAR10		
	ResNet _{1FC}	ResNet _{2FC}	ResNet _{3FC}
	90.24	90.27	88.95
	MNIST		
PlainCNN _{1FC}	PlainCNN _{2FC}	ResNet _{3FC}	
98.87	99.66	98.66	
SVHN			
ResNet _{1FC}	ResNet _{2FC}	ResNet _{3FC}	
94.77	95.29	93.05	

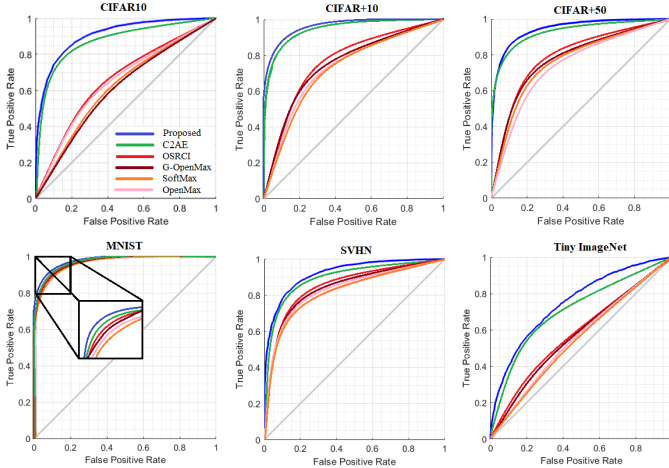


Fig. 8: AUROC performance comparison between proposed OSRNet and other methods in the literature. OSRNet outperforms all the existing methods on all six benchmark datasets.

the other hand, there is no penalty for a correct classification ($C(N|N) = C(P|P) = 0$).

$$P = TruePositive + FalseNegative$$

$$N = TrueNegative + FalsePositive.$$

A line with the slope S_{op} is dragged from the upper-left corner of the ROC plot (where $FPR = 0, TPR = 1$) down and to the right. The first intersection point of the slope line and the ROC curve is the optimal operating point. The value which ensures the optimal cut-off point is selected as the δ when OSRNet is deployed.

5. Performance Comparison

An open set recognizer performs two tasks simultaneously: it has to identify an input either as KK or UU and classify it correctly if KK. While accuracy is a good metric to gauge classification performance, UU detection performance should be evaluated on a metric that takes True Positive Rate (TPR) and False Positive Rate (FPR) into account. Therefore, we provide evaluation results separately with AUROC as the detection metric and TOP-1 accuracy as the classification metric. OSRNet outperforms other works in the literature under both metrics- AUROC (see Table 2 and Figure 8) and classification accuracy (see Table 3).

Class Conditioned Auto-Encoder (C2AE) (Oza and Patel, 2019) comes close to OSRNet in terms of AUROC performance on a number of datasets. C2AE follows a 3-stage training scheme. First, a dataset is randomly divided into D_{KK} and D_{UU} . An encoder (a CNN minus the SoftMax output) is trained on D_{KK} . A decoder is augmented to the encoder output and is trained to reconstruct any given input. The entire network (when the encoder-decoder ensemble works as one unit) is designed to reconstruct any D_{KK} instance as precisely as possible. However, it is designed to poorly reconstruct D_{UU} instances so that the reconstruction error is high for UUs at inference time. Finally, at inference time, reconstruction error is calculated for each input. D_{KK} inputs are expected to be correctly reconstructed. Therefore, the reconstruction error for D_{KK} instances should be close to zero. For D_{UU} instances, however, the reconstruction will have a significant error compared to its

Table 5: AUROC performance (%) comparison of different benchmark datasets as the base D_x for choosing D_{KUT} . The number of images inside D_x is listed in the column header and the number of images ultimately qualifying for D_{KUT} is provided inside the parenthesis in each row. Interestingly, D_{KUT} - although a subset of D_x and much smaller in size, works consistently better than using entire D_x as D_{KUT} across all four datasets.

KK	UU							
	CIFAR100		Indoor67		Caltech256		Tiny ImageNet	
	D_x (all 46k)	$D_{KUT} (> T)$	D_x (all 16k)	$D_{KUT} (> T)$	D_x (all 28k)	$D_{KUT} (> T)$	D_x (all 100k)	$D_{KUT} (> T)$
CIFAR10	86.10	89.25 (25k)	82.03	83.82 (9k)	90.40	93.15 (18k)	87.54	88.40 (64k)
CIFAR+10	-	-	83.65	85.76 (9.5k)	94.88	95.69 (19k)	88.45	91.40 (62k)
CIFAR+50	-	-	82.33	83.60 (9k)	93.50	94.60 (18k)	86.94	89.78 (60k)
Tiny ImageNet	72.06	74.55 (23k)	69.50	70.95 (7.5k)	75.70	77.10 (16k)	-	-

D_{KK} counterpart. This way, the magnitude of the error is exploited to determine whether an instance belongs to the UU or not. As advocated in Hendrycks et al. (2019), we attribute OSR-Net’s better task performance to the use of an effective, diverse, and real Known Unknown Trainer dataset over encoder-decoder based generative models.

As mentioned earlier, detecting UUs is one side of OSR. Maintaining accuracy on classifying D_{KK} images is the other side of it. Compared to the traditional ResNet_{1FC}, our modified ResNet with two FC layers (ResNet_{2FC}) performs better on OSR task (See Table 2). ResNet_{2FC} not only benefits our OSR performance, it also ameliorates the classification accuracy (see Table 3). ResNet_{2FC} performs better than ResNet_{1FC} on the standard classification task (see Table 4). We argue that the increased depth of the FC layers in ResNet_{2FC} provides richer features and boosts classification accuracy as well. However, using more than two FC layers do not work as well as using two (see our empirical analysis in Table 4).

Comparison with OOD methods. Outlier Exposure (OE) proposed in Hendrycks et al. (2019) emphasizes on training with real and diverse KU datasets. To represent outliers (when $D_{KK} \subset \text{CIFAR10}$), the work Liang et al. (2018) trains on all the images in the ‘80 million tiny image’ dataset Torralba et al. (2008) while we only use 18k images. In this case, our novelty lies in not naively using entire datasets as outliers. As for ODIN Liang et al. (2018) and Generalized ODIN Hsu et al. (2020), both use temperature scaling while the latter not requiring any additional outlier training data. However, as shown in Table 2, OSRNet performs better than the above mentioned OOD methods under the OSR evaluation protocol. We attribute this to the different loss landscapes for these two paradigms which although similar, are not exactly same Engstrom et al. (2019).

6. Discussion

To perform the OSR task, OSRNet is trained with a specially mined dataset D_{KUT} . We discussed in Section 3.2 the mining process of D_{KUT} and the type of images that work well as D_x . However, the significance of the size of D_{KUT} (or the number of images) is also worth discussing. Our experimental results show that the type of images is more important than the number of images. Our proposed method leaves only around half of the images (16k) from Caltech256 (D_x) into D_{KUT} . However, it performs better than using the entire Caltech256 (28k) as the D_{KUT} (Table 5). To understand the underlying reason behind

this, we need to go back to the conceptual illustration provided in Figure 7. In order to detect UUs at test time, the best way is to collect a set of borderline KUs and train the classifier to draw a decision boundary between this and D_{KK} . Anything beyond this decision line should be treated as unknown. Using an entire D_x set as D_{KUT} (Dhamija et al. (2018)) is not a good idea since such a D_{KUT} would contain both the borderline (circles) and far-away (triangles) images. We argue that most of the KU instances from D_x that do not make it to the D_{KUT} can be automatically detected at test time if our classifier draws a line in between D_{KUT} (borderline ones) and D_{KK} . The following section elaborates on the experimental analysis.

CIFAR100. If we use all 46k images from CIFAR100 as the D_{KUT} , the AUROC scores come out as 86.10% and 72.06% for CIFAR10 and Tiny ImageNet respectively. Whereas, if the images inducing probability greater than 80% are used in D_{KUT} , the score becomes 89.25% (25k) and 74.55% (23k) for CIFAR10 and Tiny ImageNet respectively.

Indoor67. If we use all 16k images from Indoor67 as the D_{KUT} , the AUROC scores come out as 82.03%, 83.65%, 82.33%, and 69.50% for CIFAR10, CIFAR+10, CIFAR+50, and Tiny ImageNet respectively. Whereas, if the images inducing probability greater than 80% are used as D_{KUT} , the score becomes 83.82% (9k), 85.76% (9.5k), 83.60% (9k), and 70.95% (7.5k) for CIFAR10, CIFAR+10, CIFAR+50, and Tiny ImageNet respectively.

Caltech256. If we use all 28k images from Caltech256 as the D_{KUT} , the AUROC scores come out as 90.40%, 94.88%, 93.50%, and 75.70% for CIFAR10, CIFAR+10, CIFAR+50, and Tiny ImageNet respectively. Whereas, if the images inducing probability greater than 80% are used as the D_{KUT} , the score becomes 93.15% (18k), 95.69% (19k), 94.60% (18k), and 77.10% (16k) for CIFAR10, CIFAR+10, CIFAR+50, and Tiny ImageNet respectively.

Tiny ImageNet. If we use all 100k images from Tiny ImageNet as the D_{KUT} , the AUROC scores come out as 87.54%, 88.45%, and 86.94% for CIFAR10, CIFAR+10 and CIFAR+50 respectively. Whereas, if the images inducing probability greater than 80% are used as the D_{KUT} , the score becomes 88.40% (64k), 91.40% (62k), and 89.78% (60k) for CIFAR10, CIFAR+10, and CIFAR+50 respectively.

Table 5 does not include digit-based MNIST and SVHN datasets in the KK column as such other datasets are scarcer. Non-digit datasets with natural images (e.g., Caltech256) do

Table 6: D^T_{UU} from the left out set of CIFAR-10 is the most challenging testset compared to D^T_{UUS} drawn from non-overlapping SVHN and Indoor67 testsets.

	$D_{KK} \subset \text{CIFAR10}$		
	AUROC (%)		
	D^T_{UU-C}	D^T_{UU-S}	D^T_{UU-I}
C2AE ((Oza and Patel, 2019))	89.50	92.88	88.59
OSRNet	93.15	98.30	94.95

not work well at all as the D_x for MNIST and SVHN. It can be summarized that Caltech256 performs best as D_x for mining D_{KUT} because of its similarity with D_{KK} along with class diversity.

Train and Test Data Distributions. It is possible that even after explicitly removing all the overlapping classes, there could still be an implicit overlap between D^T_{UU} and D_{KUT} because of the nature of these datasets. However, the core of our proposed method revolves around the fact that D_{KUT} lies close to the D_{KK} distribution. Therefore, our network’s decision boundary around the D_{KK} distribution is fairly tight. Hence, OSRNet is capable of successfully identifying UUs regardless of the distribution of D^T_{UU} . A conceptual illustration is provided in Figure 7. To show OSRNet performs consistently with or without any implicit overlap between D_{KUT} and D^T_{UU} , we expand our test datasets for further experimentations. In addition to the default D^T_{UU} , we test on two separate D^T_{UUS} according to the following setup:

- $D_{KK} \subset \text{CIFAR10}$ (default train split).
- $D^T_{UUS} = \text{SVHN}$ testset.
- $D^T_{UUI} = \text{Indoor67}$ testset.
- $D^T_{UUC} \subset \text{CIFAR10}$ testset (default unknown test split).
- $D^T_{UUC} \cap D_{KK} = \emptyset$.

CIFAR10 contains 10 different classes such as bird, dog and six randomly selected classes are used as the D_{KK} . Indoor67 dataset contains 67 interior classes, e.g., bedroom, office, and garage, while SVHN contains 10 classes belonging to digits (0-9). These two datasets do not visually or semantically overlap with the D^T_{UUC} . In fact, samples from both D^T_{UUS} and D^T_{UUI} are easier to identify as outliers compared to D^T_{UUC} owing to their greater distance from D_{KK} . Table 6 supports our claim, i.e., OSRNet performs better on distant and non-overlapping unknowns. On D^T_{UUS} and D^T_{UUI} , OSRNet produces 5.15% and 1.80% greater AUROC score respectively compared to D^T_{UUC} . Table 7 reinforces our argument regarding the inter distribution distance measured using Maximum Mean Discrepancy (MMD) Borgwardt et al. (2006).

MMD can approximate the distance between the underlying distribution of two image datasets based on the Reproducing Kernel Hilbert Space (RKHS) Borji (2019); Li et al. (2017). We used the final FC layer features from OSRNet Backbone to represent the dataset distributions. Let $X = \{x_1, \dots, x_{n_1}\}$ and

Table 7: Both D^T_{UUS} and D^T_{UUI} have greater distance from D_{KK} compared to the default testset D^T_{UUC} . This complements our findings in Table 6 where OSRNet performs better on distant testsets.

	$D_{KK} \subset \text{CIFAR10}$			
	$D_{KK} \rightarrow D_{KUT}$	$D_{KK} \rightarrow D^T_{UUC}$	$D_{KK} \rightarrow D^T_{UUS}$	$D_{KK} \rightarrow D^T_{UUI}$
		CIFAR10	SVHN	Indoor67
MMD	0.18	0.23	0.59	0.44

$Y = \{y_1, \dots, y_{n_2}\}$ be two datasets with distributions \mathcal{P} and \mathcal{Q} . The empirical distance between \mathcal{P} and \mathcal{Q} , according to MMD, is

$$\text{Dist}(X, Y) = \left\| \frac{1}{n_1} \sum_{i=1}^{n_1} \phi(x_i) - \frac{1}{n_2} \sum_{i=1}^{n_2} \phi(y_i) \right\|_{\mathcal{H}}$$

where \mathcal{H} is a universal RKHS Steinwart (2001), and $\phi : \mathcal{X} \rightarrow \mathcal{H}$

It is evident from Table 7 that D_{KUT} indeed resides close to D_{KK} . It is also apparent that visually and semantically distant datasets are indeed far away from D_{KK} and hence, easier to detect. This is analogous to our findings in Table 6 where OSRNet performs better on Both D^T_{UUS} and D^T_{UUI} than D^T_{UUC} . Our experimental results also complement the conceptual visualisation in Figure 7.

7. Conclusion

Open set recognition is one of the pressing issues deep image classifiers are faced with. In this work, we analyzed CNNs’ behaviour on both KK and UU datasets and proposed a network that is adept at the OSR task. Instead of using synthetic images, we have demonstrated that a trainer dataset mined from publicly available datasets can represent the unknown better. OSRNet functions as a single end-to-end unit at inference time. It outperforms contemporary OSR techniques on a number of benchmark datasets. We have also discussed the reasons behind OSRNet’s success in the given task through conceptual decision boundaries and comparative entropy analysis. There is still room for improvement in terms of generalisation of our training approach. To be more specific, we used heuristical assumptions to select a source dataset to mine the Known Unknown Trainers. We believe a distance based metric, such as Maximum Mean Discrepancy, can be used to justify the selection of a certain source dataset. This can be investigated further in future. Besides, images detected as unknowns by OSRNet can be further cognized. This will open up avenues for unsupervised image labelling as well.

References

- Bendale, A., Boulton, T.E., 2016. Towards open set deep networks, in: Proceedings of the IEEE conference on Computer Vision and Pattern Recognition (CVPR).
- Blum, A., 1992. Neural networks in C++: an object-oriented framework for building connectionist systems. John Wiley & Sons, Inc.
- Borgwardt, K.M., Gretton, A., Rasch, M.J., Kriegel, H.P., Schölkopf, B., Smola, A.J., 2006. Integrating structured biological data by kernel maximum mean discrepancy. Bioinformatics 22, e49–e57.

- Borji, A., 2019. Pros and cons of gan evaluation measures. *Computer Vision and Image Understanding (CVIU)* 179, 41–65.
- Dang, S., Cao, Z., Cui, Z., Pi, Y., Liu, N., 2019. Open set incremental learning for automatic target recognition. *IEEE Transactions on Geoscience and Remote Sensing*, 2019 .
- Deng, J., Dong, W., Socher, R., Li, L.J., Li, K., Fei-Fei, L., 2009. Imagenet: A large-scale hierarchical image database, in: *IEEE Conference on Computer Vision and Pattern Recognition (CVPR)*, pp. 248–255.
- DeVries, T., Taylor, G.W., 2018. Learning confidence for out-of-distribution detection in neural networks. *arXiv:1802.04865* .
- Dhamija, A.R., Günther, M., Boulton, T., 2018. Reducing network agnostophobia. *Advances in Neural Information Processing Systems (NIPS)* , 9157–9168.
- Dube, S., 2018. High dimensional spaces, deep learning and adversarial examples. *arXiv:1801.00634* .
- El-Sherif, E.A., Abdelazeem, S., 2007. A two-stage system for arabic handwritten digit recognition tested on a new large database., in: *Artificial Intelligence and Pattern Recognition*, pp. 237–242.
- Engstrom, L., Tran, B., Tsipras, D., Schmidt, L., Madry, A., 2019. Exploring the landscape of spatial robustness, in: *International Conference on Machine Learning (ICML)*, pp. 1802–1811.
- Ge, Z., Demyanov, S., Chen, Z., Garnavi, R., 2017. Generative openmax for multi-class open set classification. in *British Machine Vision Conference (BMVC)* .
- Geng, C., Tao, L., Chen, S., 2020. Guided cnn for generalized zero-shot and open-set recognition using visual and semantic prototypes. *Pattern Recognition* , 107–263.
- Goodfellow, I., 2016. Generative adversarial networks. *Neural Information Processing Systems (NIPS)* 2016 .
- Goodfellow, I.J., Shlens, J., Szegedy, C., 2015. Explaining and harnessing adversarial examples. in *International Conference on Learning Representations (ICLR)* .
- Grosse, K., Manoharan, P., Papernot, N., Backes, M., McDaniel, P., 2017. On the (statistical) detection of adversarial examples. *arXiv:1702.06280* .
- He, K., Zhang, X., Ren, S., Sun, J., 2016. Deep residual learning for image recognition, in: *Proceedings of the IEEE Conference on Computer Vision and Pattern Recognition (CVPR)*, pp. 770–778.
- Hein, M., Andriushchenko, M., Bitterwolf, J., 2019. Why relu networks yield high-confidence predictions far away from the training data and how to mitigate the problem, in: *Proceedings of the IEEE Conference on Computer Vision and Pattern Recognition (CVPR)*, pp. 41–50.
- Hendrycks, D., Gimpel, K., 2016. A baseline for detecting misclassified and out-of-distribution examples in neural networks. *arXiv:1610.02136* .
- Hendrycks, D., Mazeika, M., Dietterich, T.G., 2019. Deep anomaly detection with outlier exposure, in: *International Conference on Learning Representations (ICLR)* .
- Hossain, M.T., Teng, S.W., Zhang, D., Lim, S., Lu, G., 2019. Distortion robust image classification using deep convolutional neural network with discrete cosine transform, in: *2019 IEEE International Conference on Image Processing (ICIP)*, IEEE. pp. 659–663.
- Hsu, Y.C., Shen, Y., Jin, H., Kira, Z., 2020. Generalized odin: Detecting out-of-distribution image without learning from out-of-distribution data, in: *Proceedings of the IEEE/CVF Conference on Computer Vision and Pattern Recognition (CVPR)*, pp. 10951–10960.
- Krizhevsky, A., Hinton, G., 2009. Learning multiple layers of features from tiny images. in *Technical Report*, University of Toronto , 7.
- LeCun, Y., Cortes, C., Burges, C., 2010. Mnist handwritten digit database .
- Lee, K., Lee, H., Lee, K., Shin, J., 2017. Training confidence-calibrated classifiers for detecting out-of-distribution samples, in: *International Conference on Learning Representations (ICLR)* .
- Li, C.L., Chang, W.C., Cheng, Y., Yang, Y., Póczos, B., 2017. Mmd gan: Towards deeper understanding of moment matching network. *NIPS* .
- Li, X., Li, F., 2017. Adversarial examples detection in deep networks with convolutional filter statistics, in: *Proceedings of the IEEE International Conference on Computer Vision (ICCV)*, pp. 5764–5772.
- Li, Y., Maguire, L., 2010. Selecting critical patterns based on local geometrical and statistical information. *IEEE transactions on pattern analysis and machine intelligence* , 1189–1201.
- Liang, S., Li, Y., Srikant, R., 2018. Enhancing the reliability of out-of-distribution image detection in neural networks. *International Conference on Learning Representations (ICLR)* .
- Mandal, D., Narayan, S., Dwivedi, S.K., Gupta, V., Ahmed, S., Khan, F.S., Shao, L., 2019. Out-of-distribution detection for generalized zero-shot action recognition, in: *Proceedings of the IEEE Conference on Computer Vision and Pattern Recognition (CVPR)*, pp. 9985–9993.
- Neal, L., Olson, M., Fern, X., Wong, W.K., Li, F., 2018. Open set learning with counterfactual images, in: *Proceedings of the European Conference on Computer Vision (ECCV)*, pp. 613–628.
- Netzer, Y., Wang, T., Coates, A., Bissacco, A., Wu, B., Ng, A.Y., 2011. Reading digits in natural images with unsupervised feature learning. in *Advances in Neural Information Processing Systems (NIPS)* .
- Nguyen, A., Yosinski, J., Clune, J., 2015. Deep neural networks are easily fooled: High confidence predictions for unrecognizable images, in: *Proceedings of the IEEE Conference on Computer Vision and Pattern Recognition (CVPR)* .
- Oza, P., Patel, V.M., 2019. C2ae: Class conditioned auto-encoder for open-set recognition. in *Proceedings of the IEEE Conference on Computer Vision and Pattern Recognition (CVPR)* .
- Perera, P., Morariu, V.I., Jain, R., Manjunatha, V., Wigington, C., Ordonez, V., Patel, V.M., 2020. Generative-discriminative feature representations for open-set recognition , 11814–11823.
- Rudd, E., Jain, L.P., Scheirer, W.J., Boulton, T., . The extreme value machine. in *IEEE Transactions on Pattern Analysis and Machine Intelligence (PAMI)*, 2018 .
- Scheirer, W.J., Jain, L.P., Boulton, T.E., . Probability models for open set recognition. in *IEEE Transactions on Pattern Analysis and Machine Intelligence (PAMI)*, 2014 .
- Scheirer, W.J., de Rezende Rocha, A., Sapkota, A., Boulton, T.E., 2012. Toward open set recognition. in *IEEE Transactions on Pattern Analysis and Machine Intelligence (PAMI)* , 1757–1772.
- Steinwart, I., 2001. On the influence of the kernel on the consistency of support vector machines. *Journal of Machine Learning Research (JMLR)* 2, 67–93.
- Swets, J.A., 1992. The science of choosing the right decision threshold in high-stakes diagnostics. *American Psychologist* .
- Tanay, T., Griffin, L., 2016. A boundary tilting perspective on the phenomenon of adversarial examples. *arXiv:1608.07690* .
- Torralba, A., Fergus, R., Freeman, W.T., 2008. 80 million tiny images: A large data set for nonparametric object and scene recognition. *IEEE transactions on pattern analysis and machine intelligence* 30, 1958–1970.
- Vyas, A., Jammalamadaka, N., Zhu, X., Das, D., Kaul, B., Willke, T.L., 2018. Out-of-distribution detection using an ensemble of self supervised leave-out classifiers, in: *Proceedings of the European Conference on Computer Vision (ECCV)*, pp. 550–564.
- Xiao, H., Rasul, K., Vollgraf, R., 2017. Fashion-mnist: a novel image dataset for benchmarking machine learning algorithms. *arXiv:1708.07747* .
- Yoshihashi, R., Shao, W., Kawakami, R., You, S., Iida, M., Naemura, T., 2019. Classification-reconstruction learning for open-set recognition, in: *Proceedings of the IEEE Conference on Computer Vision and Pattern Recognition (CVPR)*, pp. 4016–4025.
- Zhang, H., Patel, V.M., . Sparse representation-based open set recognition. *IEEE Transactions on Pattern Analysis and Machine Intelligence (PAMI)*, 2016 .
- Zweig, M.H., Campbell, G., 1993. Receiver-operating characteristic (roc) plots: a fundamental evaluation tool in clinical medicine. *Clinical chemistry* , 561.